# Structural Properties of Weakly Segregated PS−PB Block Copolymer Micelles in *n*-Alkanes: Solvent Entropy Effects

**Reidar Lund,*,†,§ Lutz Willner,† Peter Lindner,‡ and Dieter Richter†**

*Institut für Festkörperforschung, Forschungszentrum Jülich, 52425 Jülich, Germany, and Institut Laue-Langevin, B.P. 156X, Avenue des Martyrs, F-38042 Grenoble Cedex 9, France*

*Received September 23, 2008; Revised Manuscript Received January 22, 2009*

ABSTRACT: This work reports a systematic study of the aggregation behavior and structural properties of micelles formed by a selectively deuterated *h*-polystyrene-*d*-polybutadiene (*h*-PS10-*d*-PB10, where 10 denotes the approximate block molecular weight in kilograms per mole) block copolymer in a series of *n*-alkanes, $C_nH_{2n+2}$, where $n = 7$, 10, 12, 14, 16. By applying small-angle neutron scattering (SANS) in combination with contrast variation, very detailed aspects of the micellar structure are resolved. The results show that the micelles are rather poorly segregated with a large quantity of solvent (approximately 35−55%) penetrating the core and a smaller compact corona. Interestingly, the solvent fraction in the core decreases, and the overall aggregation number increases with the size of the solvent molecules. At first sight, this is not intuitively expected because the Flory−Huggins interaction parameter, $\chi$, or the interfacial tension, $\gamma$, stay constant or are even slightly decreasing, thus suggesting that the enthalpic interactions between the core-forming PS segments and the *n*-alkanes remain unchanged or decrease. However, this behavior can be understood semiquantitatively by applying a modified mean field theory where the solvent entropy effects in both core and corona are properly taken into account. This work thus directly demonstrates that contributions of the solvent entropy to the overall free energy are important whenever the interfacial tension is low.

## 1. Introduction

The self-assembly of block copolymers in selective solvents has been a subject of significant interest over the last several decades. This is manifested in an extensive amount of theoretical and experimental work published on this topic in recent years.[1,2] The usual picture is that a typical A−B diblock copolymer spontaneously self-assembles into micelles with a structure (spherical, cylindrical, etc.) essentially depending on block copolymer molecular weight characteristics and solvent quality. Classically, the resulting polymer micelles are modeled to consist of a central meltlike core solely composed of blocks of polymer B and a corona consisting of A chains surrounded by a large fraction of solvent. In the strong segregation limit, these two domains are generally considered to be separated by a sharp interface.[3−5] This is generally achieved when the solvent is highly selective and the interfacial tension, $\gamma$, or, correspondingly, the Flory−Huggins interaction parameters between the polymer blocks, $\chi_{A-B}$, and between the B block and the solvent, ($\chi_{B-S}$), all assume large numbers. However, in reality for many important systems, the $\chi$ parameters are relatively small and comparable such that the limiting case of large segregation is not given. Nevertheless, most of the discussion in the literature presented so far does not consider this aspect in detail, and most experimental comparisons with theories have been done assuming strong segregation.

Among the typical experimentally studied block copolymer systems, only a few can be regarded as highly segregated systems. These include various poly(hydrocarbon)-poly(ethylene oxide) (PEO)-based aqueous systems such as poly(ethylene-*alt*-propylene) ((PEP)-PEO),[6−8] polybutadiene ((PB)-PEO), or polystyrene ((PS)-PEO), which are all characterized by large $\chi$ parameters. In fact, for these systems, the experimental results have shown good agreement with theoretical predictions concerning the corona structure[7,8] and scaling behavior of the micellar characteristics.[8,9] For the PS-PEO block copolymer, however, the situation is more complex because the core-forming PS block in its well-segregated pure form has a high glass-transition temperature, $T_g$. This generally requires a cosolvent to produce equilibrium structures in aqueous solutions. Consequently, the results may be influenced by the method of preparation and do not entirely reflect the equilibrium. However, as recently shown experimentally,[10−13] nonequilibrium issues are not only limited to high $T_g$ components but are also inherent for amphiphilic systems where the large interfacial tension results in very large kinetic barriers and, consequently, extremely slow or nonexistent equilibration. Therefore, from this point of view, more weakly segregated systems, where the formation rates are much faster, are preferred.

For micelles that are not strongly segregated, there has been a prominent lack of systematic studies addressing the relation between thermodynamics and structure. Weak segregation has been seen in many systems, which, for example, is reflected in a high degree of solvent penetration and intermixing with the B block in the micellar core. This has been observed by small-angle neutron and X-ray scattering (SANS/SAXS) in aqueous systems such as PEO-poly(propylene oxide) ((PPO)-PEO) micelles,[14,17] poly(butylene oxide) ((PBO)-PEO) micelles,[15] or nonaqueous systems such as polyisoprene-PS(PI-PS) micelles in *n*-decane.[16] Contrast variation and model fitting revealed that the micelles are spherical and consist of a homogeneously swollen core with approximately 15−25% solvent depending on molecular weight. The corona structure was found to depend on the composition/molecular weight of the block copolymer: a more diffuse density profile was found for asymmetric block copolymers, whereas for more symmetric compositions, the corona was homogeneous, which is similar to what has also been found for well-segregated PEP-PEO micelles.[7] Studies of PS-PI and PS-PI-PS micelles have been performed in various phthalates, which are slightly selective for PS.[18−20] By employing SAXS and SANS combined with detailed data modeling, these studies have demonstrated that depending on the alkane substitution of the phthalates, various micellar structures ranging

* Corresponding author. E-mail: reidar_lund@ehu.es.
† Forschungszentrum Jülich.
‡ Institut Laue-Langevin.
§ Present address: Donostia International Physics Center, Paseo Manuel de Lardizabal 4, 20018 Donostia-San Sebastián, Spain.

10.1021/ma8021629 CCC: $40.75 © 2009 American Chemical Society
Published on Web 03/06/2009

**Table 1. Molecular Weight Characteristics of the *h*-PS10-*d*-PB10 Block Copolymer**

| $M_n$(PSPB)[a] | $M_w/M_n$[b] | $M_n$(PS)[b] | $N_{PS}$ | $M_n$(PB)[c] | $N_{PB}$ |
|---|---|---|---|---|---|
| 22 200 | 1.03 | 10 500 | 100 | 11 700 | 195 |

[a] Membrane osmometry. [b] Size exclusion chromatography/PS calibration. [c] Calculated from $M_n$(PSPB) and $M_n$(PS10).

**Table 2. Densities and Scattering Length Densities of the *n*-Alkanes at 20 °C**

| solvent | empirical formula | $d$ (g·cm$^{-3}$) | $\rho_0$ ($10^{10}$ cm$^{-2}$) |
|---|---|---|---|
| *n*-heptane | $C_7H_{16}$ | 0.6837 | −0.547 |
| *n*-heptane-$d_{16}$ (96.2% D) | $C_7D_{15.39}H_{0.61}$ | 0.7926 | 6.061 |
| *n*-decane | $C_{10}H_{22}$ | 0.7298 | −0.489 |
| *n*-decane-$d_{22}$ (99% D) | $C_{10}D_{21.78}H_{0.22}$ | 0.8451 | 6.538 |
| *n*-dodecane | $C_{12}H_{26}$ | 0.7492 | −0.464 |
| *n*-dodecane-$d_{26}$ (99% D) | $C_{12}D_{25.74}H_{0.26}$ | 0.8631 | 6.634 |
| *n*-tetradecane | $C_{14}H_{30}$ | 0.7627 | −0.444 |
| *n*-tetradecane-$d_{30}$ (98.6% D) | $C_{14}D_{29.58}H_{0.42}$ | 0.8771 | 6.686 |
| *n*-hexadecane | $C_{16}H_{34}$ | 0.7734 | −0.429 |
| *n*-hexadecane-$d_{34}$ (99% D) | $C_{16}D_{33.66}H_{0.34}$ | 0.8895 | 6.783 |

from spherical, ellipsoidal, elongated cylinders, and even vesicular shape are formed. Although the results clearly show that small subtle changes in chemistry and thermodynamics clearly affect the structure, no quantification in terms of the thermodynamical parameters was performed. A thorough thermodynamical model was developed in a recent paper by Zhulina et al.[21] to account for structural transitions in such micelles, in particular, the experimentally observed phase behavior of various PS-PI micelles in *n*-heptane. The results showed a good agreement with the dependence of aggregation number on block molecular weights and could also account for the sphere-to-cylinder crossover, which is associated with crew-cut micelles. A similar system, PEP-PS in a series of *n*-alkane solvents, has been studied experimentally using light scattering.[22,23] These measurements have shown that the selectivity systematically increases with the carbon number, *n*, of the solvent, which is reflected in an increase in the aggregation number and a decrease in the critical micelle concentration (cmc). However, because light scattering was used in this case, no detailed structural analysis was possible.

In this work, we present a systematic study of micellar properties of a *h*-PS10-*d*-PB10 block copolymer in *n*-alkanes, $C_nH_{2n+2}$, with carbon numbers $n = 7$ (*n*-heptane), 10 (*n*-decane), 12 (*n*-dodecane), 14 (*n*-tetradecane), and 16 (*n*-hexadecane). To obtain detailed structural information by SANS, the PB-block was selectively deuterated for contrast variation. *n*-Alkanes are selective for PB such that the micelles consist of fully hydrogenated PS cores and deuterated PB coronas. By isotopic mixtures of the *n*-alkane solvents, the individual parts of the micelles were independently resolved. The characteristics of the micelles were obtained by core−shell model fits. The fit results reveal an increase in the aggregation number with increasing *n*-alkane chain length, although $\chi$ values and interfacial tensions, $\gamma$, estimated from the work of adhesion and Hildebrand's solubility parameters, are constant or even decreasing. This counterintuitive behavior can be explained by applying a mean-field-type theory[24,25] and also properly including the solvent entropy associated with the swelling of the core.

## 2. Experimental Section

**2.1. Materials.** *Polymer Synthesis and Characterization.* The *h*-PS10-*d*-PB10 block copolymer was made by sequential anionic polymerization of styrene and a mixture of 98.6% 1,3-butadiene-$d_6$ (Chemotrade, Leipzig, Germany, 98.5% D) and 1.4% 1,3-butadiene-$h_6$ (Aldrich). Therefore, the *d*-PB block is, in fact, a random copolymer of *d*- and *h*-monomers with a total degree of deuteration of 97%. The addition of the *h*-butadiene reduces the scattering length density of the *d*-PB block, allowing for complete matching of the corona by the deuterated solvents. High vacuum/break-seal techniques were applied to the polymerization to avoid termination by humidity, air, or both. We were thereby essentially following the techniques described in the literature.[26,28] The polymerization was carried out in benzene at room temperature, starting with PS and copolymerizing PB. This solvent leads to a high degree of 1,4-microstructure (93%) in the PB block. Prior to the polymerization of the second PB block, a small *h*-PS10 sample was removed from the reactor for separate characterization. This block was analyzed for molecular weight and polydispersity by size exclusion chromatography using conventional PS calibration. The molecular weight distribution of the final diblock copolymer was determined by the same method. The absolute number-average molecular weight, $M_n$, was obtained from membrane osmometry in toluene at 37 °C. A more detailed description of the preparation and characterization of PS-PB diblock copolymers can be found in ref 29. All molecular weight characteristics are summarized in Table 1.

The scattering length densities of the polymers, $\rho$, were calculated according to the general formula

$$\rho = \frac{N_A \sum_i b_i}{V} \tag{1}$$

where for the polymers, $b_i$ denotes the coherent scattering length of the *i*th atom of the repeat unit, and $N_A \approx 6.022 \times 10^{23}$ is Avogadro's number. $V$ denotes the molar volume given by $V = M/d$, where $M$ is the molecular weight of the basic repeat unit and $d$ is the density of the respective polymer. Densities of PS and *d*-PB are 1.034 g·cm$^{-3}$[45] and 0.995 g·cm$^{-3}$, respectively. The density of the deuterated polymer was calculated from the protonated materials,[45] assuming identical volumes. The scattering length densities were then calculated to be $\rho_{PS} = 1.390 \times 10^{10}$ cm$^{-2}$ and $\rho_{d\text{-PB}} = 6.471 \times 10^{10}$ cm$^{-2}$ at 20 °C.

*Solvents and Sample Preparation.* The protonated *n*-alkane solvents were purchased in p.A. quality from Aldrich. The corresponding deuterated solvents, $C_nD_{2n+2}$, where $n = 7$, 10, 12, 14, 16, with a nominal degree of deuteration between 98 and 99% were purchased from Cambridge Isotope Laboratories (Andover, Massachusetts). All solvents were used as received without further purification. The scattering length densities of the solvents were calculated according to eq 1. The densities were measured at 20 °C using a commercial U-tube Anton Paar DMA 5000 density meter. The scattering length densities of the solvent mixtures used for contrast variation were calculated according to: $\rho_0 = (1 - f_d)\rho_0(h) + f_d\rho_0(d)$, where $f_d$ is the volume fraction of deuterated solvent.

The degree of deuteration, densities, and corresponding calculated scattering length densities of the pure solvents are summarized in Table 2.

We prepared the samples for SANS measurements by dissolving the polymer at approximately 70−80 °C for 2 to 3 h until clear and homogeneous solutions were obtained. Subsequently, the samples were allowed to equilibrate by slowly cooling to room temperature. *n*-Alkanes have a finite solubility in PS, leading to a strong plastification effect where the glass-transition temperature, $T_g$, is lowered by more than 50 °C.[27] This was confirmed by earlier results of the equilibrium exchange kinetics on the same system.[37] Therefore, we can exclude any effect of the high glass transition of pure PS (about 100 °C) by this sample preparation protocol.

**2.2. Small-Angle Neutron Scattering Experiments and Data Evaluation.** The SANS measurements were carried out using the KWS-1 and KWS-2-instruments at the FRJ-2 reactor at Forschungszentrum Jülich GmbH in Germany and the D-11 instrument at Institute Laue Langevin (ILL) in Grenoble, France. The measurements were performed at several sample-to-detector distances and collimation lengths to cover an extended $Q$ range and to maintain a reasonable resolution. The wavelength was set to 7 and 6 Å in Jülich and Grenoble, respectively. For the D-11 instrument, the $Q$ range was approximately $1 \times 10^{-3} \leq Q \leq 0.3$

Å$^{-1}$, and in Jülich, it was $2 \times 10^{-3} \leq Q \leq 0.2$ Å$^{-1}$. Detector sensitivity corrections were made with Lupolen or plexi glass in Jülich, whereas water was used in Grenoble. The same materials were used as secondary standards. Empty cell scattering and the background signal arising from electronic noise, $\gamma$ radiation, and fast unmoderated neutrons were subtracted using standard procedures. The background noise was determined using cadmium (Cd) or boron carbide to block the primary beam. All background subtraction was done directly pixel by pixel on the 2D detector intensity image. After radial averaging, the intensities were treated for dead-time effects to yield the absolute normalized macroscopic differential scattering cross sections, $(d\Sigma/d\Omega)(Q)$. To keep internal consistency and to ensure that data obtained at different instruments could be compared, standard hydrogenated *n*-alkane solvents were measured at each instrument, and small errors in absolute intensities (<10−20%) were corrected.

*Fit Models for the Small-Angle Neutron Scattering Data.* For the current system where PS forms the core and PB forms the corona, the total weighted scattering amplitude can be written as

$$A(Q) = (\rho_{PS} - \rho_0)PV_{PS}A(Q)_{core} + (\rho_{PB} - \rho_0)PV_{PB}A(Q)_{shell} \quad (2)$$

Here we have introduced the scattering length density and molar volume of the different components, $\rho_j$ and $V_j$, respectively, where $j$ denotes solvent ($j = 0$), PS ($j = PS$), or PB ($j = PB$). $P$ is the aggregation number, that is, the number of polymer chains per micellar aggregate.

The total macroscopic differential scattering cross section scattering in units of reciprocal centimeters is then given by

$$\frac{d\Sigma}{d\Omega}(Q) = \frac{\phi N_A}{PV_{PS-PB}}\langle |A(Q)|^2 \rangle \quad (3)$$

where $\phi$ is the volume fraction of polymer, $N_A = 6.022 \times 10^{23}$ denotes Avogadro's number, and $V_{PS-PB} = V_{PS} + V_{PB}$ is the total molar volume of the polymer.

The scattering amplitudes, $A_i(Q)$, of core ($i$ = c) and shell ($i$ = sh), are given by the respective Fourier transformation of the real density profile ($n_i(r)$), that is

$$A_i(Q) = \exp(-(Q\sigma_c R_c)^2/4))\frac{4\pi}{C}\int_0^\infty n_i(r) r^2 \frac{\sin(Qr)}{Qr}\, dr \quad (4)$$

where $C$ is a normalization constant given by $C = 4\pi\int_0^\infty n_i(r) r^2\, dr$

The first term takes into account the smooth variation of the density at the core−corona interface by assuming a Gaussian profile of the interfacial region. (See, for example, ref 33.) In the evaluations, several functional forms of the density profile are considered. These will be discussed later in the text. To describe the scattering over the whole $Q$ range, the single chains constituting the corona visible at high $Q$ need to be taken into account. Here we use a simple parametrization based on the Beaucage form factor for chains with arbitrary statistics[34]

$$\frac{d\Sigma^{Beau}}{d\Omega_{blob}}(Q) = (\rho_{PB} - \bar{\rho}_0)^2 B\left(\frac{(\mathrm{erf}(Q\xi/\sqrt{6}))^3}{Q}\right)^{d_f} \quad (5)$$

where $B$ is an intensity prefactor proportional to the blob volume, erf($y$) is the error function, $\xi$ is the blob size, and $d_f$ is the fractal dimension that, for swollen chains, takes the value of 1.7. Note, as the error function decays to zero at $Q = 0$, this approach ensures proper normalization.

The total macroscopic differential scattering cross section is then given by

$$\frac{d\Sigma}{d\Omega}(Q) = \frac{\phi N_A}{PV_{PS-PB}}\langle |A(Q)|^2 \rangle + \frac{d\Sigma}{d\Omega}^{blob}(Q) \quad (6)$$

In the case in which the system contains particles of different size, the scattering amplitudes have to be averaged over their respective distribution

$$\langle |A(Q)|^2 \rangle = A\int_{R_{min}}^{R_{max}} |A(Q,r)|^2 p(r)\, dr \quad (7)$$

where $p(r)$ is the distribution function and $A$ is a normalization constant given by $A = 1/(\int_{R_{min}}^{R_{max}} p(r)\, dr)$. The integration limits in the numerical integration were $R_{min} = r - 5\sigma_c R_c \leq r \leq R_{max} = R_c + 5\sigma_c R_c$. The choice of the distribution functions has to be made according to the presumed particle size distribution. In this work, we chose the Schulz distribution,[35] which captures the main features of potential polydispersity effects.

The Schulz distribution is given by

$$p(r) = \frac{(z+1)^{z+1} r^z}{\langle R_c \rangle^{z+1}\Gamma(z+1)} \exp(-(z+1)r/\langle R_c \rangle) \quad (8)$$

where $\Gamma(z)$ is the gamma function and $z$ is a width parameter related to the standard deviation, $\sigma_c^p$, by

$$\sigma_c^p = \sqrt{\frac{\langle R_c^2 \rangle - \langle R_c \rangle^2}{\langle R_c \rangle^2}} = \frac{1}{\sqrt{z+1}} \quad (9)$$

Finally, the total scattering cross section was convoluted with the resolution function using the approach given by Pedersen et al.[36]

## 3. Results

Partial scattering functions were measured by SANS in three different contrasts: shell, core, and an intermediate contrast. In shell contrast, the PS core was matched by isotopic mixtures of *n*-alkanes predominantly consisting of the protonated species. In core contrast, pure deuterated solvents were used to match the shell. This was possible because the high scattering length density of *d*-PB was reduced by copolymerization with 1.4% *h*-butadiene monomer. For the intermediate contrasts, solvent mixtures were taken such that the scattering length densities were close to the average contrast of the two polymer blocks. It is worth mentioning that kinetic studies of this system performed in parallel revealed relatively fast chain exchange kinetics occurring on a time scale within seconds and hours.[37] In addition to the high reproducibility of the SANS measurements, the fast kinetics ensure that the micelles are well equilibrated, as already anticipated from the large reduction in the PS glass-transition temperature. To obtain highly detailed structural information, we analyzed the scattering data using the core−shell model described above in Section 2.2. Fitting procedures and results are presented in the following.

**3.1. Core−Shell Model Fits.** For the analysis, the polymer characteristics obtained by SEC, NMR, and density measurements were fixed parameters during the fitting procedures. These parameters were the scattering length density of each of the blocks and of the solvents, $\rho_{PS}$, $\rho_{PB}$, and $\rho_0$; the polymer block volumes, $V_{PS}$ and $V_{PB}$; and the volume fraction of the block copolymer in solution, $\phi$. Additionally, the resolution parameters of the instruments are known and were fixed. Prior to the final simultaneous fits, the scattering curves from the core and the corona were individually fitted. From these preliminary fits, all parameters were initially roughly determined.

*Micellar Core Scattering.* SANS data under core contrast in *n*-decane are representatively shown in Figure 1. Scattering curves were measured at three different concentrations at low polymer volume fractions, $\phi$ = 0.25, 0.5, and 1%. After normalization to $\phi$, all data collapse into a single curve apart from the low $Q$ region, where the intensity slightly decreases.

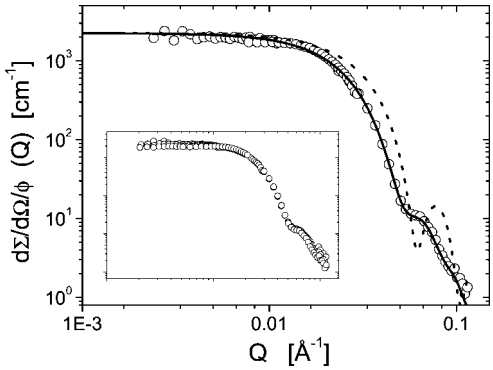


**Figure 1.** Absolute scattering cross section of *h*-PS10-*d*-PB10 micelles in *n*-decane at $\phi = 0.25\%$ under core contrast conditions (*d*-PB matched out). The dotted line displays a fit with a compact, solvent-free, monodisperse sphere model. The solid line represents a fit after allowing for solvent in the core and including a Schulz distribution for polydispersity. The data have been convoluted with the resolution function corresponding to the individual settings. The line corresponding to the lowest sample-to-detector distance is shown for clarity only. Inset: concentration dependence of the scattering cross section at $\phi = 0.25$, 0.5, and 1%. For clarity, only the lines corresponding to the lowest sample-to-detector distance is shown.

This is shown in the inset plot of Figure 1. The slight decrease in the scattering at low $Q$ is a manifestation of a structure factor contribution due to interparticle interactions. This effect could be seen in all cases, indicating a repulsive interaction between the micelles that is minor for the lowest concentration of $\phi = 0.25\%$. Therefore, all data analyses were performed at this concentration.

Initially, the core scattering was described with the scattering amplitude of a homogeneous sphere with constant density profile, $n_i(r) \approx$ constant. Inserting this into eq 4 gives

$$A_1(Q, R_c, \sigma_c)_c = \exp(-(Q\sigma_c R_c)^2/4)\frac{3}{(QR_c)^3}(\sin(QR_c) - QR_c\cos(QR_c)) \quad (10)$$

Trial fits assuming a compact core, that is, $P \approx R_c^3$, gave poor results with a clear mismatch between the forward scattering and the expected position of the minima. This is shown in Figure 1. The minimum was found to be at lower $Q$, indicating that the micellar cores are larger than expected from the volume of the *h*-PS10 polymer blocks alone. The fits could be significantly improved by allowing the core to be penetrated with *n*-alkane solvent. This was accomplished by taking $P$ and $R_c$ as free and independent parameters during the fitting routine. The mean solvent fraction in the core was then calculated according to

$$\Phi_0 = 1 - \frac{3PV_{PS}}{4\pi R_c^3} \quad (11)$$

Values for $\Phi_0$ were found to be between approximately 0.3 and 0.5 depending on the *n*-alkane solvent.

Nevertheless, the data could not be perfectly described because the oscillations of the form factors are more damped out than what is expected from the resolution effects of the instrument alone. In addition, we need to consider some kind of smearing. The fits using the Gaussian smearing parameter characterizing the core−corona interface, $\sigma_c$, yield small values on the order of 1−8%. However, although this factor produces a small smearing effect of the minima, it predominantly affects the decay at high $Q$, where high values lead to a decay that is too steep to be supported by the experimental results.

Alternatively, it is natural to consider some inherent radial distribution of the core chains. To take into account such an effect, we considered a more general Fermi−Dirac-like density profile of the core

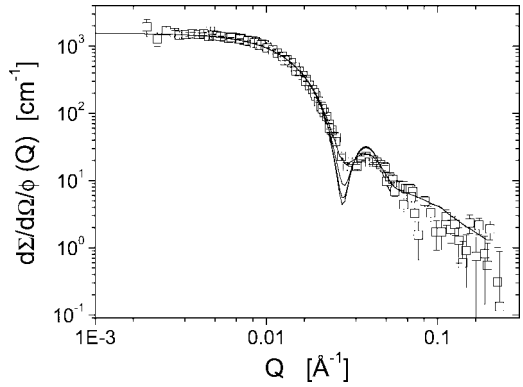


**Figure 2.** Absolute scattering cross section of *h*-PS10-*d*-PB10 micelles in *n*-heptane at $\phi = 0.25\%$ under shell contrast conditions (*h*-PS matched out). The solid lines represent a fit with a hollow sphere model including a constant density profile with a Fermi−Dirac-type cutoff function. (See the text for details.) The individual lines represent fitted curves including the convolution with the resolution function corresponding to the individual settings.

$$n_c(r) = \frac{1}{1 + \exp((r - R_c)/(\sigma'_c R_c))} \quad (12)$$

where $\sigma'_c$ is a smearing parameter.

This approach gave a very similar phenomenology as the Gaussian smearing with indistinguishable fit quality. Again, small values of $\sigma'_c$ were obtained. This suggests that the density of the core is rather compact and no evidence of uneven or inhomogeneous distribution of the solvent molecules in the core can be found.

The smearing of the minima may arise from a polydispersity of the core or deviations from the spherical symmetry induced by either strong fluctuations of the interface or a preferred ellipsoidal-like shape. To consider any such effect, we first chose a distribution function for the micellar core size and convoluted the scattering amplitude with the normalized Schulz distribution function (eq 8). Using this approach, we obtained excellent agreement with the experimental data. (See the solid line in Figure 1.) The standard deviation, $\sigma_R^p$, was found to be close to 10−15% in all cases.

Alternatively, the data can be fitted assuming that the micellar cores adopt an ellipsoidal shape. The scattering amplitude for an ellipsoid of which two of the semi axes are identical, $a = b = R$, with an axis ratio, $\epsilon$, to the third can be written as[38]

$$A_2(Q, R, \epsilon)_c = \int_0^{\pi/2} A_1(Q, R(\sqrt{\sin^2\theta + \epsilon^2\cos^2\theta}))\sin\theta\, d\theta \quad (13)$$

This approach gave the same excellent agreement as the spherical core model including the Schultz distribution. The best results were obtained for $\epsilon = 0.65$ to 0.75, that is, for oblate spheroids. Fits assuming prolate ellipsoids, $\epsilon > 1$, gave slightly worse fits. Because the aspect ratio is not very far from unity, the deviations from a spherical shape are rather small. Because of this, in addition to the fact that in some cases ellipsoids of both oblate and prolate shape could be fitted rather satisfactorily, we judge it to be more reasonable to assume a spherical shape with a certain polydispersity in size. In the remainder, we will therefore focus on the fit results obtained by the polydisperse spherical core form factor.

*Micellar Shell Scattering.* Figure 2 shows the absolute scattering cross section of *h*-PS10-*d*-PB10 micelles at $\phi = 0.25\%$ in *n*-heptane under shell contrast conditions.

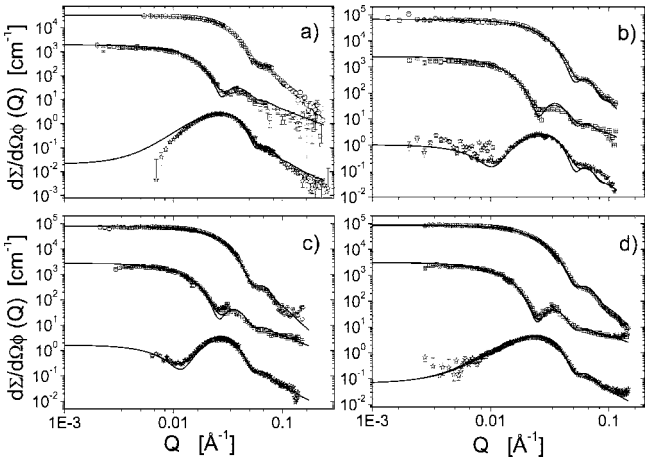


**Figure 3.** Typical core−shell model fits. Absolute scattering cross sections of *h*-PS-*d*-PB micelles in (a) heptane, (b) decane, (c) dodecane, and (d) hexadecane at $\phi = 0.25$ for different contrasts. The solid lines display fits using the core−shell model convoluted with the resolution function corresponding to the experimental settings. For better visibility, the data are shifted by a constant factor: core contrast (○), 30; shell contrast (□), 1; intermediate contrast (☆), 0.02.

The shell data were fitted with a general power law profile

$$n_{sh}(r) \approx \frac{r^{-x}}{1 + \exp((r - R_m)/(\sigma_m R_m)} \tag{14}$$

where for $x = 0$, a constant density profile is modelled, and for $x = {}^4/_3$, a starlike profile is modeled. $R_m$ denotes the micellar radius, and $\sigma_m$ denotes a smearing parameter characterizing the width of the corona−solution interface. To satisfactorily fit the data at high $Q$, the blob scattering was considered according to eqs 5 and 6. Best fits were obtained by using a constant density profile, that is, $x = 0$ and values for $\sigma_m$ between 0 and 0.1. The corresponding fit for the *h*-PS10-*d*-PB10 micelles in *n*-heptane is shown as solid lines in Figure 2.

The accuracy of the fitted parameters from the "blob scattering" term generally suffers from poor signal-to-noise ratio at high $Q$ owing to the high level of incoherent scattering. The following approximate values after fixing $\nu$ to 0.6 were obtained: a blob radius, $\xi$, of approximately 20−50 Å and B on the order of $10^{-10}$ cm$^{3-d_f}$.

*Simultaneous Fits.* Finally, the data of all three contrasts were simultaneously fitted to determine precise and consistent values for the micellar structure. The resulting fit parameters were initially roughly determined from the individual fits and could be used to get excellent results once allowing for slight variations. The scattering data for all contrasts in various *n*-alkane solvents and the corresponding fitted curves are plotted in Figure 3. The fitted parameters of the core−shell structure are summarized in Table 3.

*Temperature Dependence.* To investigate the thermal stability, we measured the *h*-PS-*d*-PB/*n*-decane system at different temperatures in core contrast. Figure 4 a shows the obtained coherent differential scattering cross sections at 10, 20, 40, and 65 °C.

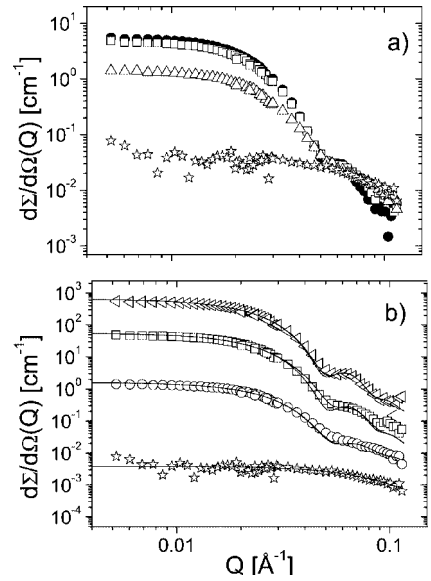


**Figure 4.** Temperature dependence of micellar structure. (a) Absolute scattering cross sections of *h*-PS10-*d*-PB10 in *n*-decane at $\phi = 0.25\%$ in core contrast at different temperatures. From top to bottom: 10, 20, 40, and 65 °C. (b) Fits to the data in a. Lines display fits using the core−shell model, the Beaucage form factor, or a sum of both. (See the text for details.) The fitted curves are convoluted by the resolution function for each setting. For better visualization, the data are shifted by a constant factor. From top to bottom: 10 °C, 100; 20 °C, 20; 40 °C, 1; 65 °C, 0.1.

The data at 10 and 20 °C, could be described by the spherical form factor including the Schultz distribution. The polydispersity in $R_c$ was found to be close to 10% as before and was fixed to this value to fit the data at 10 and 20 °C. At 40 °C, deviations from the usual homogeneous core scattering are visible. In particular, at high $Q$, the maximum disappears, and a power law with a slope of approximately 2.2 is obtained. The data could be successfully described by a general coexistence model of single chains and micelles

$$\frac{d\Sigma}{d\Omega}(Q) = \frac{\phi - \mathrm{cmc}}{PV_{PS-PB}}\langle |A(Q)|^2\rangle + \mathrm{cmc}V_{PS}\phi_{PS}(\rho_{PS} - \rho_0)^2 P(Q)_{Beau} \tag{15}$$

where $A(Q)$ is given by eq 3. $V_{PS}$ and $\phi_{PS}$ are the volume of the *h*-PS-block and the volume fraction of *h*-PS in the block copolymer, respectively. $P(Q)_{Beau}$ is the Beaucage form factor given by

$$P_{Beau}(Q) = \exp(-Q^2R_g^2/3) + (d_f/R_g^{d_f})\Gamma(d_f/2)\left(\frac{\mathrm{erf}(QkR_g/\sqrt{6})^3}{Q}\right)^{d_f} \tag{16}$$

This fit yields a cmc of ∼0.11 vol %, that is, only nearly half of the polymers exist in an aggregated state at 40 °C. Moreover, we obtain an aggregation number of $P \approx 53$ and a core radius of $R_c \approx 80$ Å. An attempt to fit the data in a limited $Q$ range ($Q \leq 0.005$ Å) without any unimer scattering yields a much lower value for the aggregation number of $P = 30$.

**Table 3. Fit Results of the *h*-PS10-*d*-PB10/*n*-Alkane System at 20 °C**

| solvent | $R_c$ (Å) | $\sigma_c$ | $\sigma_c^p$ | $R_m$ (Å) | $\sigma_m$ | $P$ | $\Phi_0$ |
|---|---|---|---|---|---|---|---|
| *n*-heptane | 83 ± 1 | 0 | 0.11 ± 0.01 | 134 ± 2 | 0.1 | 67 ± 2 | 0.53 ± 0.06 |
| *n*-decane | 91 ± 1 | 0.04 | 0.15 ± 0.01 | 144 ± 2 | 0.1 | 85 ± 2 | 0.51 ± 0.05 |
| *n*-dodecane | 88 ± 2 | 0.08 | 0.12 ± 0.01 | 148 ± 1 | 0.1 | 100 ± 1 | 0.40 ±0.08 |
| *n*-tetradecane | 90 ± 1 | 0.05 | 0.10 ± 0.05 | 154 ± 2 | 0.1 | 106 ± 2 | 0.41 ±0.04 |
| *n*-hexadecane | 90 ± 2 | 0.04 | 0.11 ± 0.07 | 150 ± 2 | 0.2 | 110 ± 2 | 0.39 ±0.07 |

**Table 4. Parameters from the Model Fitting of the *h*-PS10-*d*-PB10/*n*-Decane System at Different Temperatures**

| $T$ (°C) | $\langle R_c \rangle$ (Å) | $P$ | $\Phi_0$ |
|---|---|---|---|
| 10 | 90 ± 1 | 105 ± 4 | 0.42 |
| 20 | 86 ± 1 | 90 ± 3 | 0.45 |
| 40 | 80 ± 1 | 53 ± 2 (30)[a] | 0.58 (0.77)[a] |
| 65[b] | 21 ± 2[b] | 1 | 1[c] |

[a] Values in parentheses correspond to fits of the data at 40 °C without unimer scattering. [b] $R_g$ of the *h*-PS10-block. [c] Here we adopt the definition of $\Phi_0 \equiv 1$ when the micelles are completely dissolved and only unimers are present.

At 65 °C, the shape and intensity of the curves resemble scattering from single chains. In this case, the data could be successfully described with the Beaucage form factor alone. The volume of the polymer from the forward scattering was found to be in very good agreement with the value determined from the polymer characterization. Therefore, this parameter was held fixed to this value, $V_{PS} = 10\,150$ cm$^3$/mole, calculated from the known densities and molecular weights (Table 1). The resulting fit yields a radius of gyration of $R_g \approx 21$ Å and a fractal dimension of $d_f \approx 2.2$. All fit parameters are given in Table 4. The corresponding fits are depicted in Figure 4.

**3.2. Calculation of Interfacial Tensions and $\chi$ Parameters.** To understand the structure and aggregation behavior of the micelles, it is essential to know the relevant $\chi$ parameters and the interfacial tensions in the system.

*Calculations of Interfacial Tensions Using Fowkes' Theory.* The macroscopic interfacial tension between PS and *n*-alkanes, $\gamma_{PS-n\text{-alkane}} \equiv \gamma$, is difficult to measure directly at room temperature. Less directly, $\gamma$ can be obtained via contact angle measurements and calculation from the well-known Young's equation.[42] However, test measurements demonstrated that the contact angle method is inapplicable because high-energy surfaces such as PS are completely wetted by *n*-alkanes in a normal air atmosphere. Alternatively, $\gamma$ can be indirectly calculated from the work of adhesion, $W_a$, through

$$\gamma = \gamma_{PS} + \gamma_s - W_a \tag{17}$$

where $\gamma_s$ is the surface tension of the solvent. According to Fowkes,[44] $W_a$ can be calculated according to

$$W_a = 2\sqrt{\gamma_{PS}^d \gamma_s^d} \tag{18}$$

where $\gamma^d$ denotes the dispersion part of the surface tension.

The surface tension of PS, $\gamma_{PS}$, and its dispersion part, $\gamma_{PS}^d$, have previously been determined by measuring the contact angles of water drops on PS surfaces immersed in a series of *n*-alkanes.[43] This study yielded $\gamma_{PS} = 38.1$ mN·m$^{-1}$ and $\gamma_{PS}^d = 37.5$ mN·m$^{-1}$ and showed that $\gamma$ decreases monotonically with the length of short *n*-alkanes.

For higher *n*-alkanes, $\gamma$ was calculated using eqs 17 and 18. We took $\gamma_{PS} = 38.1$ mN·m$^{-1}$ and $\gamma_{PS}^d = 37.5$ mN·m$^{-1}$ from ref 43 and values for $\gamma_s$ for the *n*-alkanes from ref 46. We further assumed the fact that neutral, nonpolar molecules such as *n*-alkanes only interact through dispersion forces, such that $\gamma_s^d = \gamma_s$. It should be mentioned that several values for $\gamma_{PS}$ exist in the literature. Using $\gamma_{PS} = 39.4$ mNm$^{-1}$, as reported elsewhere,[45] we estimate the systematic error of $\gamma_{PS-n\text{-alkane}}$ to be about 50%. However, the trend is unaffected. The results are depicted in Table 5.

*Calculations of $\chi$ and $\gamma$ using Hildebrand's Solubility Parameter.* The interaction parameters, $\chi$, can be obtained from solubility parameter considerations using tabulated values for the cohesive energy density and Hildebrand's solubility parameters.[45,47]

**Table 5. Interfacial Tensions between PS and *n*-Alkanes Calculated from the Work of Adhesion According to Fowkes**

| *n*-alkane | $\gamma_s$ (mN·m$^{-1}$) | $W_a$ (mN·m$^{-1}$) | $\gamma$ (mN·m$^{-1}$) ± 50% |
|---|---|---|---|
| *n*-heptane | 20.14 | 54.96 | 3.28 |
| *n*-decane | 23.83 | 59.79 | 2.14 |
| *n*-dodecane | 25.4 | 61.73 | 1.77 |
| *n*-tetradecane | 26.56 | 63.12 | 1.54 |
| *n*-hexadecane | 27.47 | 64.19 | 1.38 |

**Table 6. Calculated Flory−Huggins Interaction Parameters and Interfacial Tensions between PS and *n*-Alkanes using Hildebrand's Solubility (Cohesion) Parameter for PS, $\delta_{PS} = 19.09$(MPa)$^{1/2}$[a]**

| *n*-alkane | $v_0$ (Å$^3$) | $\delta_i$ (MPa$^{1/2}$) | $\chi_{PS-n\text{-alkane}}$ | $\gamma$(mN·m$^{-1}$) |
|---|---|---|---|---|
| *n*-heptane | 243.29 | 15.3 | 0.81 | 5.7 |
| *n*-decane | 323.69 | 15.8 | 0.70 | 5.3 |
| *n*-dodecane | 377.48 | 16 | 0.65 | 5.1 |
| *n*-tetradecane | 432.17 | 16.2 | 0.61 | 5.0 |
| *n*-hexadecane | 486.10 | 16.4 | 0.58 | 4.8 |

[a] Reference lattice volume is chosen to be $v_0 = 80$ cm$^3$/mole.

The enthalpic part of the Flory−Huggins parameter, $\chi_h$, is related to the solubility parameter, $\delta$, in the following way[47]

$$\chi_h = \frac{V_0}{k_b T}(\delta_p - \delta_0)^2 \tag{19}$$

where $\delta_p$ and $\delta_0$ are the solubility parameters of the polymer and the solvent, respectively. $v_0$ is the elemental "lattice" volume. This latter parameter is ambiguous and depends on the definition of the lattice system. Here we define this quantity to be the mean segment volume of the PB and PS repeat units, that is, $v_0 \approx (100 + 60)/2 = 80$ cm$^3$/mole.

The total Flory−Huggins parameter, $\chi$, is given by

$$\chi = \chi_h + \chi_s \tag{20}$$

where $\chi_s$ denotes the entropic part. $\chi_s$ usually has a value between 0.3 and 0.4 for neutral polymers. We chose $\chi = 0.34$, which is found to be the typical common value.[47]

The calculated parameters are shown in Table 6. The $\chi$ parameter slightly decreases ($\chi \approx 0.8$ to 0.6) within the homologous series of *n*-alkanes.

Provided that the components are well segregated,[50] the interfacial tension can then be estimated from $\chi$ using the theory of Helfand and coworkers[48]

$$\gamma = \frac{k_b T}{a^2}\left(\frac{\chi}{6}\right)^{1/2} \tag{21}$$

where $a$ is the lattice length, which we again calculate from the mean unit segment volume using $a \approx (v_0)^{2/3} = 26$ Å.

As shown in Table 6, $\gamma$ remains approximately constant, even though we see a slight tendency for it to decrease as a function of the *n*-alkane length, following the same trend as that found before.

By analogy to this, the Hildebrand approach can also be used to estimate $\chi$ parameters between the solvophilic PB and the solvent, $\chi_{PB-n\text{-alkane}}$. The results, again assuming an equal reference length, are given in Table 7.

## 4. Discussion

**4.1. Micellar Structure.** *Aggregation Behavior.* The results show that the *h*-PS10-*d*-PB10 block copolymer forms well-defined spherical micelles in *n*-alkanes where the structure is independent of the polymer concentration for polymer volume fractions of $\phi = 0.25$ to 1% at 20 °C. This also implies that the

**Table 7. Calculated Flory−Huggins Interaction Parameters between PB and *n*-Alkanes ($\chi_{PB-n\text{-alkane}}$) using Hildebrand's Solubility (Cohesion) Parameter for PB, $\delta_{PB} = 17.19$ (MPa)$^{1/2}$[a]**

| *n*-alkane | $v_0$ (Å$^3$) | $\delta_i$ (MPa$^{1/2}$) | $\chi_{PB-n\text{-alkane}}$ |
|---|---|---|---|
| *n*-heptane | 243.29 | 15.3 | 0.45 |
| *n*-decane | 323.69 | 15.8 | 0.39 |
| *n*-dodecane | 377.48 | 16 | 0.38 |
| *n*-tetradecane | 432.17 | 16.2 | 0.37 |
| *n*-hexadecane | 486.10 | 16.4 | 0.36 |

[a] Reference lattice volume is chosen to be $v_0 = 80$ cm$^3$/mole.

cmc of the polymer is well below the investigated dilute concentration regime at this temperature. Upon heating, as seen in Figure 4, the micelles gradually dissolve into unimers.

The SANS data clearly exclude any bimodal distribution including the formation of anomalous large micelles observed in earlier studies of similar diblock copolymers. (See ref 39 and references therein.) In any case, in a systematic study by Lodge and coworkers,[39] this phenomenon has later been shown to be provoked by the presence of finite amounts of homopolymer impurities that act as a sort of "nucleation" or aggregation sites. The absence of anomalous micellization behavior confirms SEC data of the *h*-PS10-*d*-PB10 block copolymer from which the presence of homopolymer could be unambiguously excluded.

In the next paragraph, we discuss the subtle effects of the *n*-alkane solvent on the structural properties of the micelles.

*Dependence of Aggregation Number on n-Alkane.* Upon changing the solvent, the data show a weak but significant increase in the aggregation number, $P$, and the core radius, $R_c$, as the carbon number, $n$, of the *n*-alkane solvent increases.

The distinct increase in $P$ with the size of the solvent molecules, as shown in Figure 5, is in accordance with earlier findings.[22,23] However, recalling that $\chi_{PS-n\text{-alkane}} \approx 0.6$ to 0.8 and is thus slightly decreasing with carbon number within the homologous series of *n*-alkanes, this is rather surprising. Also, a slight decrease in the interfacial tension with the length of the *n*-alkanes (Tables 5 and 6) leaves the observed increase in $P$ intriguing. Usually one expects that the aggregation number monotonously increases with $\gamma$, as observed for segregated micelles.[8] Theories predict a power-law-like relation of the form $P \approx \gamma^x$, where $x$ is a power law exponent, for example, taking the value $x = 1$ in the mean field model[4] and $x = {}^6/_5$ from the scaling model for starlike micelles.[5]

The same trend was observed for similar PS-PEP micelles where $P$ was observed to increase by approximately 40% from *n*-hexane to *n*-hexadecane.[22,23] This trend was attributed to a decreasing solvent power of the *n*-alkanes; however, as seen in this study, this does not seem to be the case. Before discussing this rather intriguing aggregation behavior in more detail, we

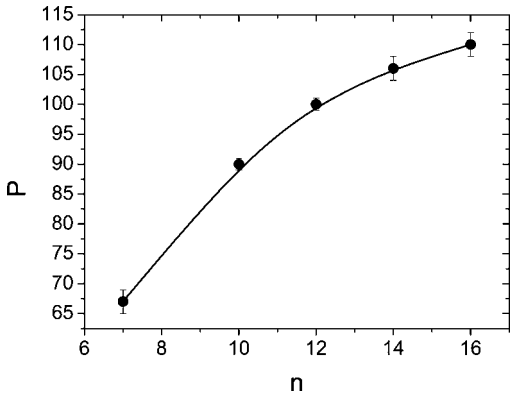


**Figure 5.** Aggregation number, $P$, of the *h*-PS10-*d*-PB10/*n*-alkane micelles versus carbon number, $n$, of the *n*-alkanes at 20 °C. The line serves as a guide to the eye only.

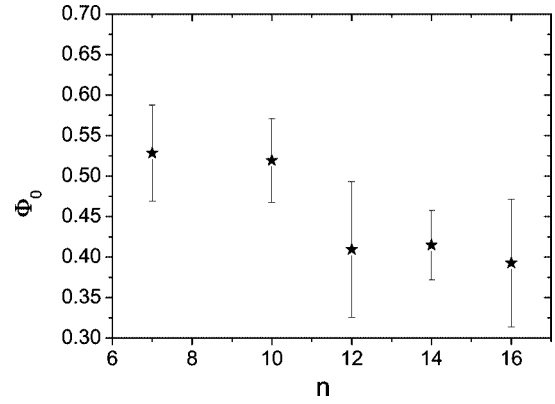


**Figure 6.** Solvent fraction inside the micellar cores, $\Phi_0$, versus carbon number, $n$, of the *n*-alkane solvent.

will first need to discuss the inherent structural details of these micelles.

*Swelling of Micellar Core.* The model fits to the scattering data reveal significantly swollen cores and a homogeneous density distribution within the core region. The solvent fraction, $\Phi_0$, slightly but systematically decreases with increasing *n*-alkane length from about 53 vol % in *n*-heptane to approximately 39 vol % in *n*-hexadecane, as shown in Figure 6. Significantly swollen cores were also observed for PS40-PI40 and PS40-PI80 block copolymer micelles in *n*-decane by Pedersen et al.[16] They found that the micellar cores contain 16 and 23% *n*-decane, respectively.

As before for the aggregation number, the decreasing solvent fraction is rather unexpected and cannot be understood on the basis of the interfacial tension alone. Because $\gamma$ stays essentially constant or slightly decreases, one would rather expect an increase in $\Phi_0$ with the *n*-alkane length.

To compare the solubility of *n*-alkanes in PS in a micellar state and in the normal bulk state, test experiments were performed where *h*-PS10 homopolymer was saturated with hexadecane and allowed to dissolve in the bulk phase upon heating the sample above the glass-transition temperature, $T_g$. The results show that this solvent fraction was less than 7 to 8%. Apparently, the capability of PS to solubilize *n*-alkanes is significantly larger inside a micellar core than in the bulk state.

The small interfacial tensions ($\gamma \approx 1$ to 5 mN·m$^{-1}$) imply rather low incompatibility between PS and *n*-alkanes. This gives rise to fluctuations of the core−corona interface, which probably are reflected in the effective polydispersity parameters. The existence of such fluctuations has unambiguously been shown in a recent study of segregated block copolymer melts where the amplitudes were about 1 to 2 nm.[52] These fluctuations may distort the spherical symmetry, leading to some apparent ellipsoidal structures as seen in microemulsion systems.[38] It may further explain the difficulty of distinguishing between polydisperse spheres and ellipsoids in the fitting. Consequently, we can attribute the apparent polydispersity in $R_c$ to fluctuations. Unfortunately, such shape fluctuations cannot be decoupled from potential polydispersity effects of $P$. Nevertheless, we can calculate typical amplitudes if we assume that the interfacial fluctuations can be described using the capillary wave dynamics[51,52]

$$\sigma_{CW}^2 = \frac{k_B T}{2\pi\gamma} \ln\left[\frac{l_{max}}{l_{min}}\right] \tag{22}$$

where $l_{max} = R_c$ and $l_{min}$ are the maximal and minimal length scales in the system. The minimal fluctuation can be estimated from the intrinsic roughness due to competition between the entropy of mixing and the unfavorable enthalpic cost. The latter

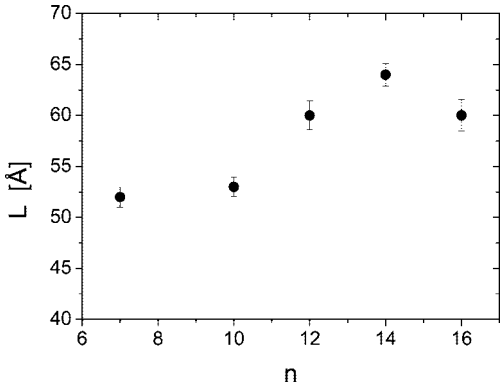


**Figure 7.** Corona thickness, $L$, defined as $L = R_m - R_c$, as a function of the carbon number, $n$, of the $n$-alkane solvents.

can be estimated by the Helfand−Tegami theory assuming, for the sake of simplicity, strong segregation

$$\sigma_{HT} = 2\sqrt{\frac{b_{PS}^2 + b_s^2}{12\chi}} \tag{23}$$

Here we take as an estimate $b_{PS} = 11$ Å[45] and $b_s \equiv V_0^{1/2} = 5.2-7.8$ Å, depending on the solvent. We then obtain $\sigma_{HT} \approx 7$ Å, which can be regarded to be the minimal length scale of the fluctuations, that is, $l_{min} = \sigma_{HT}$. Inserting this into eq 22, we obtain a fluctuation amplitude of 7−11 or 11−13 Å, depending on which values of $\gamma$ are taken: those from the Fowkes' approach (Table 5) or those from the Hildrebrand solubility parameter approach (Table 6), respectively. This give relative roughnesses, $\sigma_{CW}/R_c$, of about 6−11%. Compared with the values of the width of the Schulz distribution, $\sigma_c^p \approx 10\%$ obtained from SANS, we observe a very good agreement. Therefore, we can conclude that the fluctuations due to the low interfacial tension between PS and the solvents leads to an apparent polydispersity in the micellar sizes.

**4.2. Corona Structure.** Judging from the small values of the Gaussian smearing parameter, $\sigma_c$, the interface between the core and corona is well defined with very small interpenetration of *h*-PS10 and *d*-PB10 polymeric blocks. The internal structure of the corona can, in all cases, be described by a constant density profile with a smooth cutoff of approximately 10%. By defining the size of the corona, $L$, to be $L = R_m - R_c$, values between 52 and 64 Å are calculated, showing a slight increase in $L$ with increasing carbon length of the solvent. This is demonstrated in Figure 7.

The corona thickness can be compared with chain dimensions for linear PB chains if we assume $\theta$ conditions

$$R_g^2 = C_\infty M m_0^{-1} l_0^2/6 \tag{24}$$

where $C_\infty = 5.6$[53] is the characteristic ratio and $m_0 = 14.5$ g/mol is the average molecular weight per backbone bond of length $l_0 \approx 1.5$ Å for polybutadiene with 93% 1,4-microstructure. This gives an estimate of $R_g$ of about 41 Å and an end-to-end distance of $R_e = R_G(6)^{1/2} = 100$ Å. Compared with the unperturbed chain dimensions of PB, the corona size in the micelles appears to be rather unstretched. This can probably be directly related to the $\chi_{PB-n\text{-Alkane}}$ values (Table 7) that are in the range of 0.45 to 0.36; that is, the system is not far from the $\theta$ conditions. The resulting low degree of stretching becomes even more evident if one compares it with the dimensions encountered in strongly segregated micelles, that is, micelles with strong excluded volume interactions. For example, for PEP−PEO micelles in aqueous solutions, the PEO chains are larger than the characteristic end-to-end distance and, with respect to this, stretched by a factor of 1.5 to 1.7.[6,8] It is further interesting to note that even though the stretching of the coronal chains is significantly different, the structure as well as the mean volume fraction of the corona of the present micelles ($\eta = PV_{PB}/(4\pi/3(R_m^3 - R_c^3) \approx 0.18$ to 0.21) is very similar to that of aqueous PEP5-PEO5 micelles ($\eta \approx 0.25$).[6,7] This shows that the excluded volume effects are significantly stronger and prevail up to much larger concentrations for PEO in water. This is also reflected in much larger values for the second virial coefficient, $A_2$, for the PEO/water system where $A_2$ is on the order of $10^{-3}$ cm$^3$·mol/g$^2$.[8] By low-angle laser light scattering (LALLS), we found within experimental error constant values of about $3 \times 10^{-4}$ cm$^3$·mol/g$^2$ for PB in *n*-alkanes irrespective of the solvent length.

*Comparison with Theory.* Summarizing the structural properties, we see that the micelles can be described as being weakly segregated. This is reflected in a swollen micellar core and a rather compact unextended corona. Because the dimensions of the coronal chains are comparable to the corresponding PB chains under unperturbed ($\theta$) conditions, we can assume that contributions to the total free energy of micellization arising from chain−chain correlations in the corona are negligible. Therefore, it is reasonable to discuss our results within the classical mean-field theory of Leibler, Orland, and Wheeler,[24] which was later modified for asymmetric block copolymers by Balsara et al.[25]

Within the framework of this theory, the total free energy can be written as a sum of three contributions: the free energy of a micelle, $F_{micelle}$, the mixing term of free block copolymers and solvent, $F_{mix}$, and finally, the entropic term describing the gas of micelles and block copolymers, $S_m$. In $k_bT$ units, this can be written as

$$F_{total} = \frac{\phi\zeta}{PN} F_{micelle} + F_{mix} - TS_m \tag{25}$$

where $\zeta$ is the fraction of block copolymers in the micellar state. The individual terms can be written as

$$F_{mix} = (1 - \xi\phi\zeta)\left(\frac{\lambda \ln(\lambda)}{N} + (1 - \lambda)\frac{\ln(1 - \lambda)}{s} + \chi\frac{\lambda}{1 + f}(1 - \lambda)/(1 + f)\right) \tag{26}$$

where $\xi = (f + \eta)/(\eta(f + 1))$, $N = N_A + N_B$ is the total number of polymer segments, $f = N_A/N_B \equiv N_{PB}/N_{PS}$, and $\lambda$ is the unimer concentration, and

$$S_m/k_b = -\left(\frac{\phi\zeta}{PN}\ln(\xi\phi\zeta) + \frac{1 - \xi\phi\zeta}{\xi PN}\ln(1 - \xi\phi\zeta)\right) \tag{27}$$

The micellar free energy, $F_{micelle}$, can be approximated to consist of mainly three terms

$$F_{micelle} = F_{core} + F_{shell} + F_{int} \tag{28}$$

Within the classical Leibler, Orland, and Wheeler mean field theory, the free energy is mainly dominated by the balance between stretching and swelling of the polymer chains and the interfacial energy. Here the interactions between the coronal chains are assumed to be zero, whereas the interactions between the two blocks are implicitly assumed to be equal to those between the solvent and B (PS) block. However, to take into account swelling of the micellar core, we need to modify the theory by introducing a Flory−Huggins expression describing the enthalpic and entropic interactions between the solvent molecules and the polymer segments within the core. This can be done by writing

$$F_{\text{core}} = \frac{3}{2}P\left(\frac{R_c^2}{N_B a^2} + \frac{N_B a^2}{R_c^2} - 2\right) + \frac{4\pi R_c^3}{3a^3}\left(\Phi_0 \frac{\ln(\phi_0)}{N_0} + \Phi_0(1 - \Phi_0)\chi\right) \quad (29)$$

where $N_0$ is the number of solvent segments. The contribution from the shell takes the form

$$F_{\text{shell}} = \frac{3}{2}P\left(\frac{R_{\text{corona}}^2}{N_B a^2} + \frac{N_B a^2}{R_{\text{corona}}^2} - 2\right) + \frac{4\pi(R_m^3 - R_c^3)}{3a^3}\frac{(1 - \eta)\ln(1 - \eta)}{N_0} \quad (30)$$

The interfacial energy for a swollen core (assuming equal composition at surface and volume) must be written as

$$F_{\text{int}} = \frac{4\pi R_c^2}{a^2}\sqrt{\frac{\chi}{6}}(1 - \Phi_0) \quad (31)$$

The thermodynamical equilibrium can then be found by minimizing eq 25 numerically under the condition of preservation of volume (incompressibility): $R_c = (3PV_{PS}/(4\pi(1 - \Phi_0)))^{1/3}$ and $R_m^3 - R_c^3 = 3PV_{PB}/(4\pi\eta)$. At first, we compared the experimental data with the original theory where solvent in the core is excluded by setting $\Phi_0 \equiv 0$ in eqs 25−31. The expression for the free energy was minimized with respect to three free parameters, $P$, $\eta$, and $\zeta$, as a function of the input parameters, $N$, $f$, and $\chi$, using the direct numerical minimization routine "E04CCF" from NAG. This input parameters was then varied, and the theoretically calculated output was then iteratively fitted to the corresponding experimental values for $P$ and $\eta$ according to a least-squares minimalization procedure (Marquardt−Levenberg routine). Because the basic lattice site volume and also, consequently, $\chi$ are rather arbitrary in such mean field models and are not naturally given (note that the lattice size, $a$, scales out in the above expressions). Therefore we defined a floating parameter, unit, and mapped the number of solvent segments according to: $N_0 = n \cdot \text{unit}$. Using a mean volume of 80 cm$^3$/mole between PS and PB, we expect unit to be about 20/80 ≈ 0.25 using the known densities for the $n$-alkanes. Nevertheless, because the mapping of experimental parameters to the theoretical lattice parameters is not trivial, we initially kept unit as a free parameter. However, it was found that this parameter was rather ambiguous where many pairs of $\chi$ and unit could fit the data. With respect to $\eta$, unit mainly affected the absolute value, which intrinsically is not very well defined because we have a radial dependence on the coronal chain distribution. We therefore chose to fix unit at 0.25 but kept a scaling constant to fit $\eta$, that is, $\eta \rightarrow \eta \cdot C$. The results of a simultaneous fitting of both $P$ and $\eta$ using $N = 274$ and $f = 1.15$ are shown as dotted lines in Figure 8. The resulting fit gave $\chi = 0.62$ and a slight scaling factor of $C = 1.3$. As seen, the trend represented by the increase in $P$ with $n$ is qualitatively fitted, however, the predicted increase is much weaker. In any case, the calculations show an important result: the size and aggregation number of the micelles change with the volume of the solvent molecules. The predicted change in the swelling of the corona seems to be somewhat larger than what is observed.

Therefore, we repeated the calculations for micelles with swollen cores ($\Phi_0 \neq 0$), now considering four free variables: $\Phi_0$ in addition to $P$, $\eta$, and $\zeta$. The calculations and fitting procedure were repeated in the same manner as before, this time fitting the theoretical output to three experimental parameters, $P$, $\Phi_0$, and $\eta$, simultaneously. Again, to map the experimental values properly with respect to $\Phi_0$, we found it to be necessary to introduce a scaling value $\Phi_0 \rightarrow \Phi_0 \cdot D$. The results are given in Figure 8b.

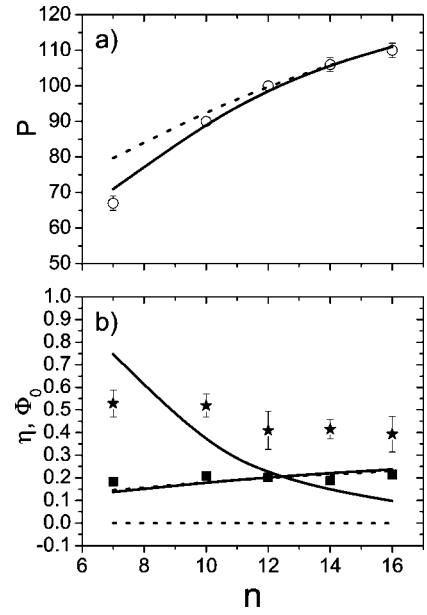


**Figure 8.** Comparison of fit results of the thermodynamical model and experimental data for (a) aggregation number, $P$. (b) Solvent fraction in the core, $\Phi_0$ (★), and mean polymer fraction in the corona, $\eta$ (■), for the $h$-PS10-$d$-PB10/$n$-alkane system. The dashed lines represent simultaneous fit calculations of the original Leibler, Orland, and Wheeler mean field theory. The solid lines display results of a modified theory where the solvent entropy is taken into account.

Here we obtained an interaction parameter of $\chi \approx 0.67$. The scaling factors were found to be $C \approx 1.8$ for the polymer fraction in the corona, and $D \approx 2.9$ scales the theoretically found solvent fraction in the core to the experimental one; that is, the theory predicts lower $\Phi_0$ and $\eta$ than those found experimentally.

As seen, the data corresponding to the modified theory allowing solvent in the core seems to describe the data for the aggregation number very well. It is also encouraging to see that the resulting $\chi$ parameters (0.62 to 0.67) agree well with what has been previously estimated using the solubility parameter approach (0.8 to 0.6) once the reference lattice volume is chosen to be the same. The theory also describes the overall trend observed for $\eta$ and $\Phi_0$ relatively well, although the absolute values are not reproduced. In addition, the decrease in the solvent fraction in the core seems to be overestimated. The reason for this behavior is likely to come from the mapping of theoretical versus experimental parameters and deviations from mean field theory. In particular, it is likely that assuming no interactions between coronal chains is an oversimplification. Nevertheless, the results nicely show that the data can be at least semiquantitatively explained by a simple mean field approach. More importantly, both experiments and calculations show that the solvent entropy plays an important role in the aggregation behavior of block copolymer micelles. Within the weak segregation limit, a fine balance of translational entropy and enthalpic repulsions will control the swelling and penetration of solvent molecules in the core and coronal part of the micelles. This, in turn, will affect balance between the interfacial energy favoring micellization and the unfavorable entropic forces associated with the stretching of chains in the micelles.

## 5. Concluding Remarks

In conclusion, we have seen that the $h$-PS10-$d$-PB10 block copolymer spontaneously self-assembles to form rather poorly segregated micelles in $n$-alkanes. A detailed comparison of

structural data obtained by highly accurate contrast variation SANS experiments reveals that the micelles contain a large number of solvent molecules homogeneously distributed in the core. Both the core and coronal part are best described by a scattering model that assumes almost constant density profiles. Interestingly, we observe that the aggregation number increases with the size of the *n*-alkane, whereas the solvent fraction in the core decreases. Intuitively, one would attribute this effect to a trend that higher *n*-alkanes are poorer solvents for the core-forming polystyrene. A detailed comparison with the thermodynamical interaction parameter and interfacial tension, however, shows that, surprisingly, these are almost constant or even decreasing within the homologous series of *n*-alkanes. As we have seen, this behavior can be semiquantitatively explained by employing a modified version of the mean field approach of Leibler, Orland, and Wheeler properly taking into account the solvent entropy in both core and corona. This work thus shows the importance of solvent translational entropy on the micellization behavior of block copolymer micelles whenever the system is weakly segregated, that is, when the interfacial tension and the $\chi$ parameters are small.

**Acknowledgment.** We acknowledge support of the European Community within the SoftComp Network of Excellence (NoE) program. We gratefully acknowledge the kind help and support from Dr. Michael Monkenbusch for the implementation of numerical routines.

## References and Notes

(1) See, for example: Hamley, I. W. *The Physics of Block Copolymers*; Oxford University Press: New York, 1998.
(2) *Amphiphilic Block Copolymers*; Alexandridis, P., Lindman, B., Eds.; Elsevier: Amsterdam, 2000.
(3) Halperin, A.; Tirrell, M.; Lodge, T. P. *Adv. Polym. Sci.* **1992**, *100*, 31.
(4) Nagarajan, R.; Ganesh, K. *J. Chem. Phys.* **1989**, *90*, 5843.
(5) Halperin, A. *Macromolecules* **1987**, *20*, 2943.
(6) Poppe, A.; Willner, L.; Allgaier, J.; Stellbrink, J.; Richter, D. *Macromolecules* **1997**, *30*, 7463.
(7) Willner, L.; Poppe, A.; Allgaier, J.; Monkenbusch, M.; Lindner, P.; Richter, D. *Europhys. Lett.* **2000**, *51*, 628.
(8) Lund, R.; Willner, L.; Stellbrink, J.; Radulescu, A.; Richter, D. *Macromolecules* **2004**, *37*, 9984.
(9) Förster, S.; Zisenis, M.; Wenz, E.; Antonietti, A. *J. Chem. Phys.* **1996**, *104*, 9956.
(10) Willner, L.; Poppe, A.; Allgaier, A.; Monkenbusch, M.; Richter, D. *Euro Phys. Lett.* **2001**, *55*, 667.
(11) Lund, R.; Willner, L.; Stellbrink, J.; Lindner, P.; Richter, D. *Phys. Rev. Lett.* **2006**, *96*, 068302.
(12) Lund, R.; Willner, L.; Dormidontova, E. E.; Richter, D. *Macromolecules* **2006**, *39*, 4566.
(13) Jain, S.; Bates, F. S. *Macromolecules* **2004**, *37*, 1511.
(14) Liu, Y.; Chen, S. H.; Huang, J. S. *Macromolecules* **1998**, *31*, 2236.
(15) Castelletto, V.; Hamley, I. W.; Pedersen, J. S. *J. Chem. Phys.* **2002**, *117*, 8124.
(16) Pedersen, J. S.; Svaneborg, C.; Almdal, K.; Hamley, I. W.; Young, R. N. *Macromolecules* **2003**, *36*, 416.
(17) Pedersen, J. S.; Gerstenberg, M. C. *Colloids Surf., A* **2003**, *213*, 175.
(18) Lodge, T. P.; Xu, X.; Ryu, C. Y.; Hamley, I. W.; Fairclough, J. P. A.; Ryan, A. J.; Pedersen, J. S. *Macromolecules* **1996**, *29*, 5955.
(19) Pedersen, J. S.; Hamley, I. W.; Ryu, C. Y.; Lodge, T. P. *Macromolecules* **2000**, *33*, 542.
(20) Bang, J.; Jain, S.; Li, Z.; Lodge, T. P.; Pedersen, J. S.; Kesselman, E.; Talmon, Y. *Macromolecules* **2006**, *39*, 1199.
(21) Zhulina, E. B.; Adam, M.; LaRue, I.; Sheiko, S. S.; Rubenstein, M. *Macromolecules* **2005**, *38*, 5330.
(22) Quintana, J. R.; Villacampa, M.; Munos, M.; Andrio, A.; Katime, I. A. *Macromolecules* **1992**, *25*, 3125.
(23) Quintana, J. R.; Villacampa, M.; Munos, M.; Andrio, A.; Katime, I. A. *Macromolecules* **1992**, *25*, 3129.
(24) Leibler, L.; Orland, H.; Wheeler, J. C. *J. Chem. Phys.* **1983**, *79*, 3550.
(25) Balsara, N. P.; Tirell, M.; Lodge, T. P. *Macromolecules* **1991**, *24*, 1975.
(26) Morton, M.; Fetters, L. J. *Rubber Chem. Technol.* **1975**, *48*, 359.
(27) Kambour, R. P.; Gruner, C. L.; Romagosa, E. E. *J. Polym. Sci.* **1973**, *11*, 1879.
(28) Hadjichristidis, N.; Iatrou, H.; Pispas, S.; Pitsikalis, M. *J. Polym. Sci., Part A: Polym. Chem.* **2000**, *38*, 3211.
(29) Gohr, K.; Schärtl, W.; Willner, L.; Pyckhout-Hintzen, W. *Macromolecules* **2002**, *35*, 9110.
(30) Dozier, W. D.; Huang, J. S.; Fetters, L. J. *Macromolecules* **1991**, *24*, 2810.
(31) Kaya, H.; Willner, L.; Allgaier, J.; Stellbrink, J.; Richter, D. *Appl. Phys. A: Mater. Sci. Process.* **2002**, *74*, S499.
(32) Kaya, H. Ph.D. Thesis, Universität Münster, **2003**.
(33) Pedersen, J. S.; Gerstenberg, M. C. *Colloids Surf., A* **2003**, *213*, 175.
(34) Beaucage, G. *J. Appl. Crystallogr.* **1996**, *29*, 134.
(35) Sheu, E. *Phys. Rev. A* **1992**, *45*, 2428.
(36) Pedersen, J. S.; Posselt, D.; Mortensen, K. *J. Appl. Crystallogr.* **1990**, *23*, 321.
(37) Lund, R.; Willner, L.; Richter, D.; Iatrou, H.; Hadjichristidis, N.; Lindner, P. *J. Appl. Crystallogr.* **2007**, *40*, s327.
(38) Arleth, L.; Pedersen, J. S. *Phys. Rev. E* **2001**, *63*, 061406-1.
(39) Lodge, T. P.; Bang, J.; Hanley, K. J.; Krocak, J.; Dahlquist, S.; Sujan, B.; Ott, J. *Langmuir* **2003**, *19*, 2103.
(40) Kotlarchyk, M.; Chen, S. H. *J. Chem. Phys.* **1983**, *79*, 2461.
(41) Zimm, B. H. *J. Chem. Phys.* **1948**, *16*, 1093.
(42) Hiemenz, P. C.; Rajagopalan, R. *Principles of Colloid and Surface Chemistry*, 3rd ed.; Marcel Dekker: New York, 1997.
(43) Qin, X.; Chang, W. V. *J. Adhes. Sci. Technol.* **1995**, *9*, 823.
(44) Fowkes, F. M. *J. Phys. Chem.* **1962**, *66*, 382.
(45) *Polymer Handbook*; Brandrup, J., Immergut, E. H., Eds.; Wiley: New York, 1975.
(46) *Handbook of Chemistry and Physics*; Weast, R. C., Ed.; CRC Press: Cleveland, OH, 1975.
(47) van Krevelen, D. W.; Hoftyzer, P. J. *Properties of Polymers: Their Estimation and Correlation with Chemical Structure*, 2nd ed.; Elsevier Scientific Pub. Co.: Amsterdam, 1976.
(48) Helfand, E.; Tagami, Y. *J. Polym. Sci., Part B: Polm. Phys.* **1971**, *9*, 741.
(49) Helfand, E.; Sapse, A. M. *J. Chem. Phys.* **1975**, *62*, 1329.
(50) Because it is known that *n*-alkanes have a significant solubility in PS (see, e.g., ref 43), this assumption may be questioned.
(51) Sferrazza, M.; Xiao, C.; Jones, R. A. L.; Bucknall, D. G.; Webster, J.; Penfold, J. *Phys. Rev. Lett.* **1997**, *78*, 3693.
(52) Lund, R.; Willner, L.; Alegría, A.; Colmenero, J.; Richter, D. *Macromolecules* **2008**, *41*, 511.
(53) Fetters, L. J.; Hadijichristidis, N.; Lindner, J. S.; Mays, J. W. *J. Phys. Chem. Ref. Data* **1994**, *23*, 619.
(54) Pipich, V.; Schwahn, D.; Willner, L. *J. Chem. Phys.* **2005**, *123*, 124904.

MA8021629